Biological Trace Element Research
https://doi.org/10.1007/s12011-019-01679-6

Iron-Induced Apoptotic Cell Death and Autophagy Dysfunction in Human Neuroblastoma Cell Line SH-SY5Y

Jyotirmoy Rakshit[1] · Arijit Mallick[1] · Susmita Roy[1] · Arpita Sarbajna[2] · Moumita Dutta[2] · Jaya Bandyopadhyay[1]

Received: 23 November 2018 / Accepted: 14 February 2019

Abstract

Iron accumulation plays a major role in neuronal cell death which has severe effects on mental health like neurodegenerative disorders. The present work aims to explore the involvement of molecular pathways involved in iron-mediated neuronal cell death using Ferric Ammonium Citrate (FAC) as a source of iron to treat neuroblastoma SH-SY5Y cells. In this study, it was found that cytotoxicity induced by iron treatment is highly correlated with enhanced intracellular reactive oxygen species (ROS) generation and loss of mitochondrial integrity. Appearance of early and late apoptotic cells with altered nuclear morphology and increased expression of effector proteins, i.e., cleaved Caspase 3 and cleaved PARP (Poly-ADP-ribose Polymerase), clearly confirmed iron-induced apoptotic cell deaths. Furthermore, excess accumulation of acidic vesicles and microtubule-associated protein 1 light chain 3 (LC3) puncta and LC3II/I expressions were observed. Simultaneously, ultrastructural studies of SH-SY5Y cells demonstrated the accumulation of a large number of autophagosomes, autophagic vacuolization, and swollen mitochondria which further confirmed the induction of autophagy concomitant with mitochondrial damage. Furthermore, increased incorporation of lysosome-specific dye, LysoTracker Deep Red, and the red fluorescence retention of LC3-GFP-RFP constructs indicates the incomplete autophagy or autophagy dysfunction due to altered lysosomal activity. Hence, the present work unveiled the interruption in autophagy progression caused by the plausible suppression of lysosomal activity due to iron treatment resulting in autophagic cell death in SH-SY5Y cell lines. In general, both apoptotic and autophagic pathways were prominent and each of the pathways played their prospective roles, in iron-mediated neuronal cell death.

Keywords Autophagy · Autophagic cell death (ACD) · Apoptosis · Ferric Ammonium Citrate (FAC) · SH-SY5Y · Lysosomal activity

Introduction

A progressive loss of functional neurons may cause retrogressive effects widely known as neurodegeneration. Amidst different molecular pathways being inaccurately regulated during neurodegeneration, one of the major molecular pathways is autophagy lysosomal pathway (ALP). Autophagy is a natural process through which unnecessary and dysfunctional components of the cell undergo an ordered process of destruction/degradation and is later recycled [1]. It is the foremost catalytic pathway maintaining cellular homeostasis. Hence, different neurodegenerative phenomena like aggregation and overexpression of α-synuclein are the aftermaths of autophagy dysfunction [2]. This pathway is a double-edged sword which plays a crucial role in both neuroprotection and neurotoxicity. Defects in autophagic clearance have been seen responsible for the progression of Parkinson's disease (PD) and other neurological disorders [3, 4].

Among other factors affecting neuronal deaths, imbalances of iron concentrations or iron dyshomeostasis are the causal reasons for the generation of reactive oxygen species (ROS), thus resulting in various neurodegenerative diseases like Parkinson's disease (PD), Alzheimer's disease (AD), Friedreich ataxia, and Huntington's disease [5, 6]. Furthermore, iron accumulation has been found to be the leading cause of neurodegeneration. In a rotenone-induced model of PD, the iron chelator, deferoxamine (DFO), enhances the

✉ Jaya Bandyopadhyay
jaya.bandyopadhyay@wbut.ac.in;
jaya.bandyopadhyay@gmail.com

[1] Department of Biotechnology, Maulana Abul Kalam Azad University of Technology, West Bengal, NH 12, Haringhata, West Bengal 741249, India

[2] Division of Electron Microscopy, ICMR-National Institute of Cholera and Enteric Diseases, Beliaghata, Kolkata, West Bengal 700010, India

Published online: 05 March 2019

progression of autophagy by stabilizing Hypoxia-inducible factor-1α (HIF-1α) and DFO is known to inhibit the rotenone-mediated apoptotic pathways [7]. On the other hand, autophagy inhibition is a therapeutic strategy against intracerebral iron overload. Increased ratio of LC3II/LC3I and accumulation of autophagic vacuoles cause autophagic cell deaths in intracranial hemorrhage, wherein iron plays a significant role. Thus, chelation of lysosomal iron has been observed to inhibit the H_2O_2 insult as demonstrated in SH-SY5Y cells by inhibiting autophagy [8, 9]. The physiological concentration of iron, being a potent modulator of autophagic events, is known to be maintained by Ferritin which stores unused iron and maintains iron homeostasis through ALP [10]. Thus, deregulated iron homeostasis may result in an interrupted autophagic flux and thereby causing deleterious effects on neuronal physiology.

Controversy still exists over the fact that whether inhibition or progression of autophagic flux is neuroprotective because there exists plenty of increasing evidences which depict the involvement of autophagy dysfunction associated with different neurological disorders. Especially, deposition of autophagosome marker LC3II in postmortem brain of PD and AD patients has proven to be the hallmark of incomplete autophagy [11]. Hence, the present study is particularly aimed at revealing the predominant role of autophagy in iron-induced neuronal deaths and the molecular mechanisms involved thereof by iron deposition. This study shows the occurrence of autophagy augmentation in a dose-dependent manner by FAC treatment and subsequent decline in cell viability, along with an increase in LC3II expression with enhanced apoptotic cell population. In summary, the present study substantiates involvement of autophagic flux during iron-mediated neuronal cell deaths and further establishes the probable suppression of the lysosomal activity in particular within the process.

Materials and Methods

Materials

Ferric Ammonium Citrate (FAC), Acridine Orange (AO), Dimethyl sulfoxide (DMSO), 2′,7′-dichlorofluorescin diacetate (DCFDA), Hoechst 33258, and Chloroquine (CQ) were purchased from the Sigma Aldrich (St Louis, MO, USA). [3-(4,5-dimethylthiazol-2-yl)-2,5-di-phenyl-tetrazolium bromide] (MTT) was obtained from Hi Media, India. All cell culture ingredients were purchased from Gibco BRL (Grand Island, NY, USA). SH-SY5Y cells (ATCC CRL-2266) were purchased from ATCC (American Type Cell Culture). LysoTracker Deep Red was purchased from Invitrogen Inc. (Carlsbad, CA, USA). Apoptosis detection kit was obtained from Cayman Chemical (Ann Arbor, MI, USA). Western blot antibodies were purchased from Abcam (Cambridge, UK).

Cell Culture and Treatment

A human neuroblastoma cell line, SH-SY5Y, was maintained in Dulbecco Modified Eagle Medium (DMEM) supplemented with 10% heat-inactivated Fetal Bovine Serum (HIFBS) and 1% penicillin-streptomycin as described. Cells were maintained in a humidified chamber at 37 °C in the presence of 5% CO_2. One hundred millimolars FAC stock was prepared in incomplete media under aseptic condition and added into the cell culture medium at the time of treatment as per required volume to achieve the respective concentrations of 1 mM, 2.5 mM, and 5 mM, respectively and continued the incubation for another 48 h.

Cell Viability Assay

Cell viability was determined by the conventional MTT (3-[4, 5-dimethylthiazol-2-yl]-2, 5-diphenyl tetrazolium bromide) reduction assay. Briefly, 5×10^4 cells were cultured in each well of 96 well plates for 24 h, followed by treatment of the cells with increasing concentrations of FAC for another 48 h. After the completion of incubation, MTT (0.5 mg/ml) was added in each well and incubated for an additional 4 h at 37 °C. Dark blue–colored formazan crystals formed on intact cells were further solubilized in dimethyl sulfoxide and absorbance was measured at 570 nm in a Microplate Reader (iMARK™, Bio-Rad Laboratories, Hercules, CA, USA). Results were expressed as percentages of reduced MTT, assuming the absorbance of control cells as 100%.

Measurement of Intracellular Reactive Oxygen Species (ROS)

In order to monitor intracellular accumulation of ROS, the fluorescent cell-permeable dye (2′, 7′-dichlorofluorescein diacetate) (DCFDA) was used. Briefly, following deacetylation within the cell, the dye binds with the intracellular radicals thus generated in a quantitative manner and is converted into its fluorescent product DCF. For the purpose, following 24 h of FAC treatment, cells were harvested and resuspended in 1× PBS (Phosphate Buffer Saline, 0.02 M, pH 7.4). DCFH-DA solution (10 μM) was added to the suspension of the cells (2×10^5/ml), and the mixture was further incubated for 30 min at 37 °C. Cells were then washed twice and resuspended in 1× PBS and the fluorescence intensity was measured spectrofluorimetrically (Perkin-Elmer LS-55) with excitation and emission wavelengths of 485 nm and 530 nm, respectively.

Measurement of Mitochondrial Membrane Potential (MMP)

MMP was determined by the fluorescent probe Rhodamine-123 Chloride (Cayman, USA) (Rh-123). Following FAC treatment, for the prescribed time, cells were incubated in the presence of 10 μg/ml Rh-123 for 15 min in the dark. After, the incubation cells were washed with 1× PBS and observed under fluorescence microscope (Leica DM 1000, Wetzlar, Germany). Fluorescence intensity of captured images was analyzed by Image J software.

Microscopic Analysis of Morphology and Autophagy Induction

Cells were cultured in six well plates for morphological analysis following the prescribed treatments with FAC. For bright-field microscopy, cells were observed under × 40 objective of an inverted fluorescent microscope (EVOS FL, Invitrogen, Carlsbad, CA, USA). Fifty micrograms per milliliter Hoechst stain for 15 min was used to determine the nuclear morphology under × 40 objective of an inverted fluorescent microscope (EVOS FL, Invitrogen, Carlsbad, CA, USA). To monitor the autophagic flux following FAC treatments for 48 h, Acridine Orange solution was added in a final concentration of 1 μg/ml and incubated for an additional 15 min. Following incubation, cells were washed and resuspended in 1× PBS, and subsequently visualized and analyzed under the × 40 objective of a fluorescent microscope (Leica DM 1000, Wetzlar, Germany). LysoTracker Deep Red was used (final concentration of 1 μg/ml for 1 h) to monitor lysosomal activity. Lysosomes were visualized and analyzed under × 40 objective of an inverted fluorescent microscope (EVOS FL, Invitrogen, Carlsbad, CA, USA).

LC3-GFP Transfection for Monitoring Autophagy Induction

To monitor the progression of autophagy, 3×10^5 cells/well were seeded on six well plate. After achieving the desired confluency, LC3-GFP construct (Addgene no. 22405) was used for transfection subsequently followed by FAC treatments for an additional 48 h. Following completion of treatments, images were visualized and captured under fluorescence microscope (× 40) (EVOS FL, Invitrogen, Carlsbad, CA, USA).

Ultrathin Sectioning and Transmission Electron Microscopy

Following a 48-h incubation with 5 mM FAC, SH-SY5Y cells were harvested and fixed with 3% glutaraldehyde in 0.1 M sodium cacodylate buffer for 4 h. Subsequently, a secondary fixation was conducted with 1% Osmium tetroxide, followed by dehydration with ascending grades of acetone, and finally embedded in Agar 100 resin and polymerization at 60 °C. The ultrathin sections (40–50 nm) of the cells were obtained using a Leica Ultracut UCT ultramicrotome (Leica Microsystems, Germany), picked up on nickel grids, and dual-stained with 2% aqueous uranyl acetate and 0.2% lead citrate. The sections were visualized under a FEI Tecnai 12 Biotwin transmission electron microscope (FEI, Hillsboro, OR, USA) at an accelerating voltage of 100 kV.

RFP-GFP-LC3B Transfection for Monitoring Autophagy Progression

To monitor the progression of autophagy, 3×10^5 cells were seeded on coverslips. After achieving the desired confluency, a Premo™ Autophagy Tandem Sensor RFP-GFP-LC3B Kit (Invitrogen) was used for transfection of LC3B following the manufacturer's protocol which was subsequently followed by FAC treatments for an additional 48 h. Following completion of treatments, images were visualized and captured under a fluorescence microscope (× 40) (EVOS FL, Invitrogen, Carlsbad, CA, USA).

Measurement of Apoptosis

The presence of apoptotic cells were analyzed by Annexin V-FITC Apoptosis detection kit (Cayman, USA) as per the manufacturer's instructions. Briefly, 5×10^5 cells/well in a six well plate were cultured in the absence and presence of FAC. Cells were then harvested and washed with PBS. Following two washes with Annexin V binding buffer (10 mM HEPES/NaOH, pH 7.4, 140 mM NaCl, 2.5 mM $CaCl_2$), cells were resuspended in the same buffer and Annexin V-FITC/PI mixture (1:1) was added as per the manufacturer's instructions. The cells were incubated for 15 min in the dark at 37 °C and after a final wash with Annexin V binding buffer, 10,000 cells were analyzed in a flow cytometer (FACS Verse, Becton Dickinson, San Jose, CA, USA). Acquisition was performed on 10,000 gated events. Data were analyzed using either histogram or quadrant plot with FACS Diva software (BD Biosciences, San Jose, CA, USA).

Western Blot Analysis

Cells were lysed in Radio Immuno Precipitation Assay (RIPA) Buffer (Sigma Aldrich, St Louis, MO, USA) supplemented with 1 mM Phenylmethane Sulfonyl Fluoride (PMSF) (Sigma Aldrich, St Louis, MO, USA) and 1 mM protease inhibitor cocktail (Amresco Inc., Cleveland, OH, USA) on ice for 30 min and centrifuged at 12,000 rpm for 20 min. Supernatants were collected, and equal amounts (50 μg/well) of proteins were separated on a 12% SDS PAGE and

transferred to Polyvinylidene difluoride (PVDF) (Millipore Sigma, Burlington, MA, USA) membranes. The membranes were incubated in primary antibodies (1:500 to 1:1000 dilution) specific for active caspase-3 (ab2302), cleaved PARP1 (ab32064), LC3I/II (ab128025), p62 (ab56416), Beclin1 (ab62557), and β-actin (ab8227), respectively followed by Alkaline Phosphatase (AP) conjugated secondary antibodies (1:5000 dilution). Respective protein targets were identified and visualized using NBT/BCIP (Amresco Inc., Cleveland, OH, USA) reagent. Protein-level expression analysis was conducted using a Bio-Rad Gel Doc imaging system (Hercules, CA, USA) with the Quantity One 1-D Analysis Software. Fold changes in signal intensities compared with the control levels at the same time points were further represented.

Statistical Analysis

Each experiment was performed at least three times and in duplicate and all results were expressed as Mean ± SD. Statistical analyses were performed by one-way ANOVA followed by Kruskal Wallis test (wherever applicable), using Graph Pad Prism software, version 5 (GraphPad Software Inc., San Diego, CA, USA).

Results

Effect of Iron on Cell Viability and Morphology

Reduced cell viability with increasing doses of FAC was assessed by MTT assay (Fig. 1a) and morphological alterations were clearly observed by bright-field phase contrast microscopy (Fig. 1b). There was no significant loss of cell viability and morphological changes in 1 mM of FAC treatment but significant loss of cell viability with altered morphology was observed in ≥ 2.5 mM of FAC treatment in SH-SY5Y cells for 48 h. With increasing doses of FAC, SH-SY5Y cells were rounded up and the intercellular connections were lost due to the loss of neuritis.

Iron-Induced Intracellular ROS Generation

Intracellular ROS generation was increased in SH-SY5Y cells exposed to FAC as compared with the untreated cells. In 2.5 mM and 5 mM FAC treatments, there were significant increases in ROS generation ($P < 0.01$ and $P < 0.001$, respectively) (Fig. 2).

Iron Reduced Mitochondrial Membrane Potential

Maintaining integrity of mitochondrial membrane or mitochondrial membrane potential (MMP) is an important phenomenon for cell viability. Dysfunctional mitochondria or altered MMP caused irreversible apoptotic cell death. Here, MMP was significantly decreased in 2.5 mM ($P < 0.01$) and 5 mM ($P < 0.001$) FAC-treated SH-SY5Y cells (Fig. 3).

Cellular Apoptosis Induced by Iron

FAC treatment increased the cellular apoptosis as compared with the untreated cells. For 2.5 mM and 5 mM FAC treatments, there was a significant ($P < 0.01$ and $P < 0.001$, respectively)

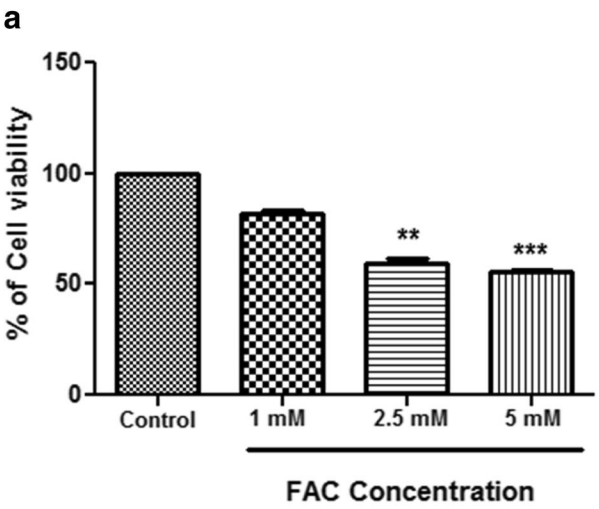

Fig. 1 Cytotoxic effect of FAC on SH-SY5Y cells. **a** Increasing concentrations of FAC (1 to 5 mM) caused SH-SY5Y cell deaths as determined by MTT assay for cell viability. The values were expressed as mean ± SD of three independent experiments [$^{**}P < 0.01$, $^{***}P < 0.001$ as compared with the untreated group (Control)]. **b**

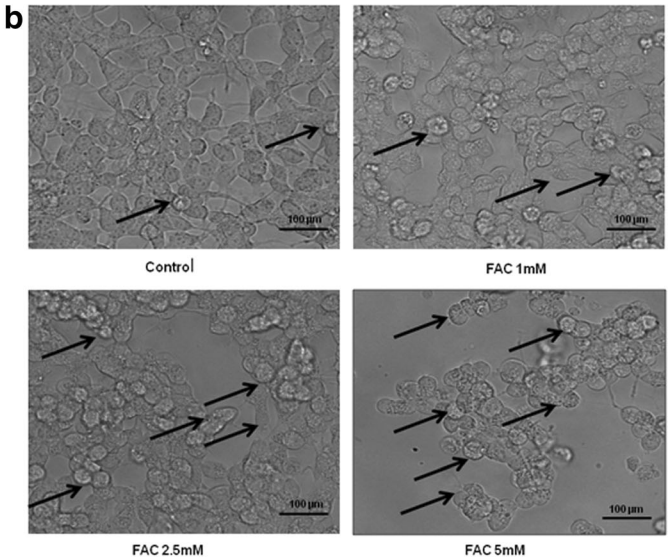

Morphological evaluation of SH-SY5Y cells with increasing FAC concentrations was made through microscopic observations (scale bar = 100 µm). Black arrows indicated shrinkage of cells with decreased neuritis extension as a measure of cell death

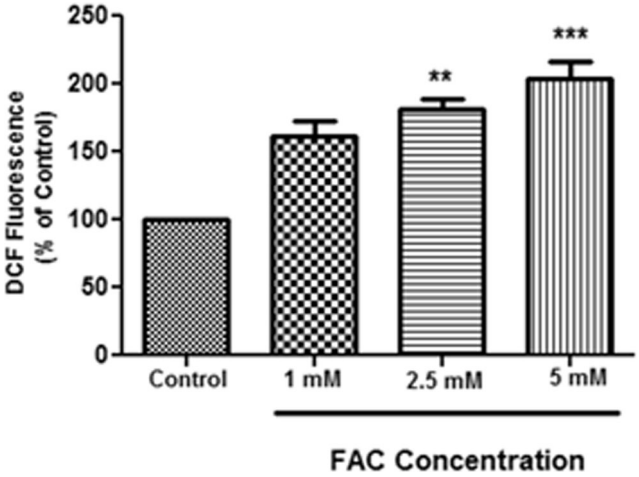

Fig. 2 Determination of ROS generation with increasing concentrations of iron. DCFDA assay was performed to determine the intracellular ROS generation. Twenty-four hours of treatment of SH-SY5Y with different concentrations of FAC, i.e., 2.5 mM and 5 mM FAC treatments, respectively caused a significant increase in ROS generation (expressed as DCF fluorescence). The values were expressed as mean ± SD of three independent experiments [$^{**}P < 0.01$, $^{***}P < 0.001$ as compared with the untreated group (Control)]

increase in both early and late apoptotic cell populations (Fig. 4a). Increasing number of condensed and fragmented nuclei as a consequence of increasing FAC treatments was also evident of apoptotic cell deaths (Fig. 4b). There was also significant upregulation of cleaved caspase 3 and cleaved PARP, the proteins that are better known as effectors for apoptotic progression (Fig. 4c). The expression of cleaved caspase 3 and cleaved PARP were significantly increased in both 2.5 mM FAC ($P < 0.01$) and 5 mM FAC ($P < 0.001$) treatments as compared with the untreated SH-SY5Y cells.

Iron-Induced Autophagy and Autophagic Flux Blocked in SH-SY5Y Cell

AO staining was used to identify the cells containing AVOs (Fig. 5a). A methachromatic shift of AO from green to red fluorescence due to the excess accumulation of low pH autophagosome, an apparent indication of autophagy induction, was thereby observed. This observation was further confirmed by the transient transfection of LC3-GFP vector construct in SH-SY5Y cells followed by the increasing doses of FAC treatments (Fig. 5b). LC3-GFP puncta formation was augmented with increased FAC treatments. In immunoblot analyses, there were increased expressions of Beclin1, LC3II, and p62 which are responsible for autophagosome formation (Fig. 6a). LC3II is an autophagosome-specific protein and it is degraded during lysosomal hydrolysis. When the fusion between autophagosome and lysosome is inhibited or the lysosomal activity is disrupted, LC3II gets deposited as a consequence. This is due to the fact that not degradation but LC3II production occurs. In order to check whether the autophagy block indeed caused the increase in LC3II level, SH-SY5Y cells were co-

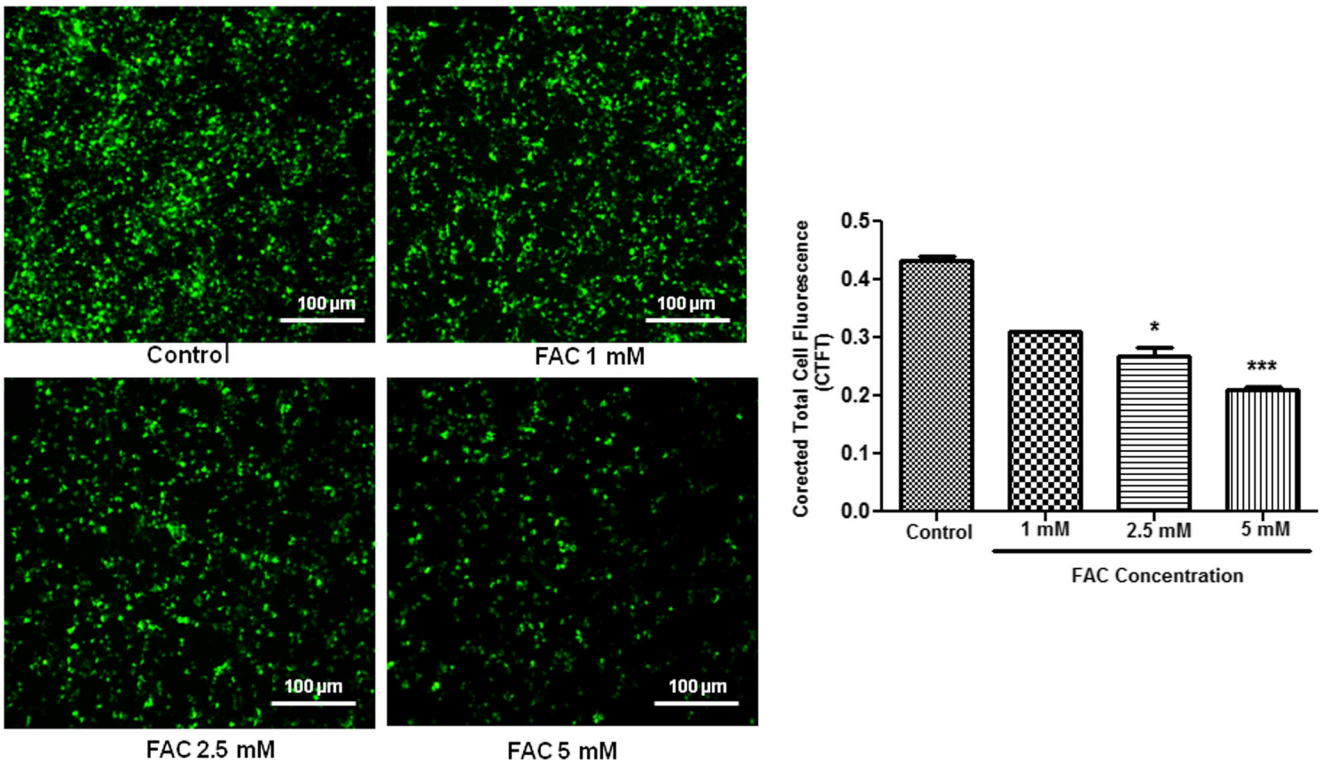

Fig. 3 FAC treatment decrease the MMP of SH-SY5Y cell: RH-123 staining was used to determine the MMP by measuring fluorescence intensity. The values were expressed as mean ± SD of three independent experiments [$^{*}P < 0.01$, $^{***}P < 0.001$ as compared with the untreated group (Control)]

a

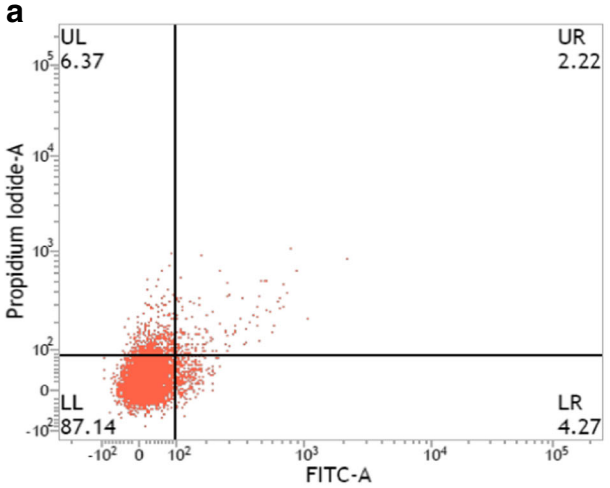

FAC 2.5 mM

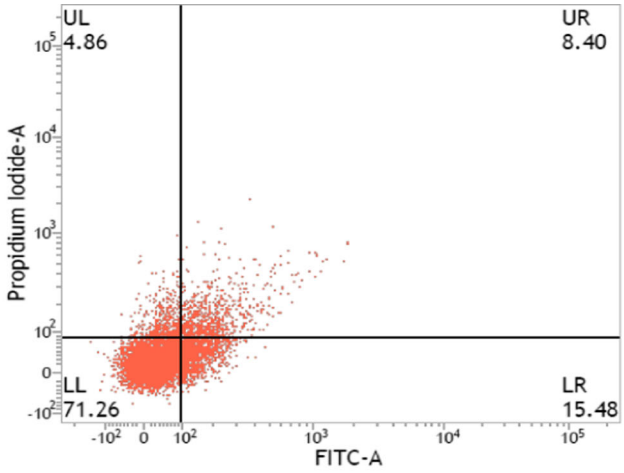

FAC 1 mM

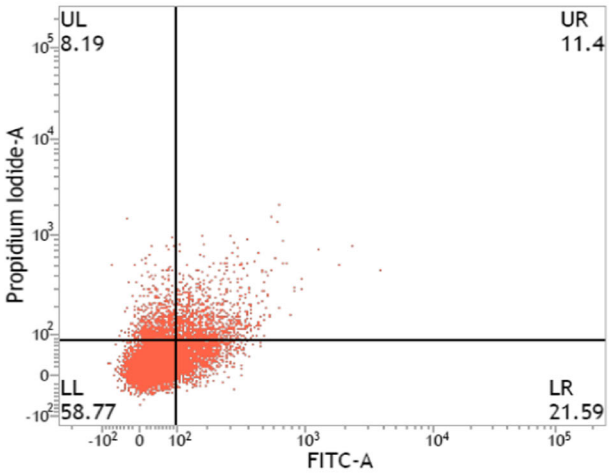

Control

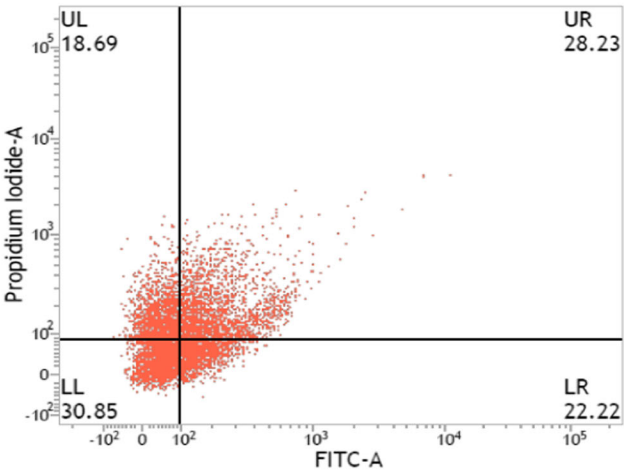

FAC 5 mM

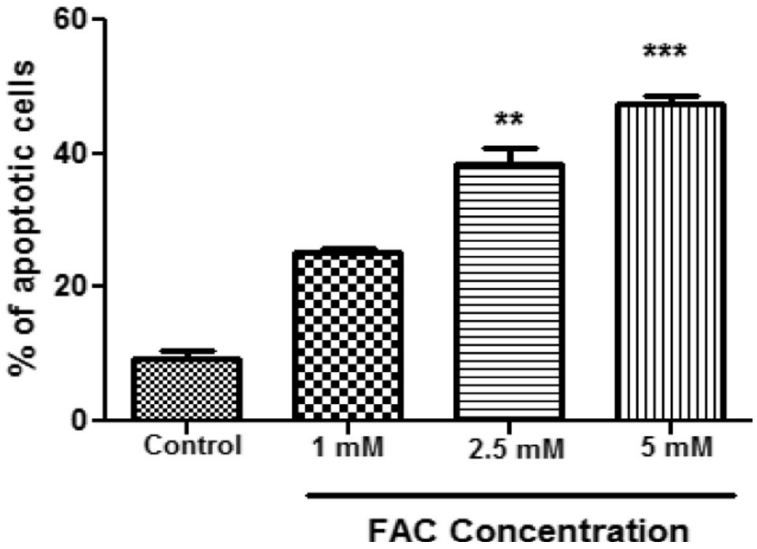

◀ **Fig. 4** Analysis of FAC-mediated neuronal apoptosis. **a** Annexin V- and PI-stained cells were analyzed by FACS. Population of early and late apoptotic cells (sum of upper right and lower right quadrants) increased with increasing concentration of FAC. 2.5 mM and 5 mM FAC treatments caused a significant increase in apoptotic cells compared with the untreated group (Control). The values were expressed as mean ± SD of three independent experiments [$^{**}P < 0.01$, $^{***}P < 0.001$ as compared with the untreated group (Control)]. **b** FAC treatment induced the apoptotic nuclear morphology in SH-SY5Y cell (white arrows). FAC-treated cells containing large number of fragmented nuclei ($n = 3$). **c** FAC treatment increased the expression of cleaved caspase 3 and cleaved PARP as compared with the untreated cells. The values were expressed as mean ± SD of three independent experiments [$^{*}P < 0.05$, $^{**}P < 0.01$, $^{***}P < 0.001$ as compared with the untreated group (Control, C)]

treated with FAC and chloroquine (CQ), a lysosome inhibitor. It was observed that LC3II levels remain unchanged in CQ co-treatment with FAC as compared with CQ treatment alone (Fig. 6b). In addition, ultra structural analysis of SH-SY5Y cells further confirmed FAC-mediated autophagy induction through excess accumulation of autophagic vacuoles (AVs), and early/late autophagosomes in comparison with the control (untreated) SH-SY5Y cells (Fig. 7). Moreover, swollen mitochondria as a consequence of FAC treatment were clearly visible in the cytoplasm of treated cells whereas very few number of early autophagosomes (APs) and regular mitochondria were observed in the cytoplasm of control cells.

Hence, it was confirmed that there was no further progression of autophagy following autophagosome formation. To check whether the lysosomes are functional or non-functional, the cells were labeled with LysoTracker Deep Red (Fig. 8a). Labeling experiments clearly revealed the presence of acidic vesicles which got accumulated in a concentration-dependent manner of FAC. Besides, a similar phenomenon was observed when cells were treated with lysosomal inhibitor CQ. Furthermore, to confirm the deposition of LC3II as a consequence of inhibition of lysosomal activity, SH-SY5Y cells were transfected with LC3-GFP-RFP Tandem reporter constructs followed by different doses of FAC. It was eventually observed that the red fluorescence was essentially overriding the green fluorescence in comparison with the untreated cells (Fig. 8b). This phenomenon was further observed for CQ-treated cells which finally supports the fact that iron induces autophagy block or prevent the progression of autophagy by inhibiting the lysosomal activities.

Discussion

Iron is a crucial trace metal for any physiological system. Excess iron or imbalance in iron turnover may cause different

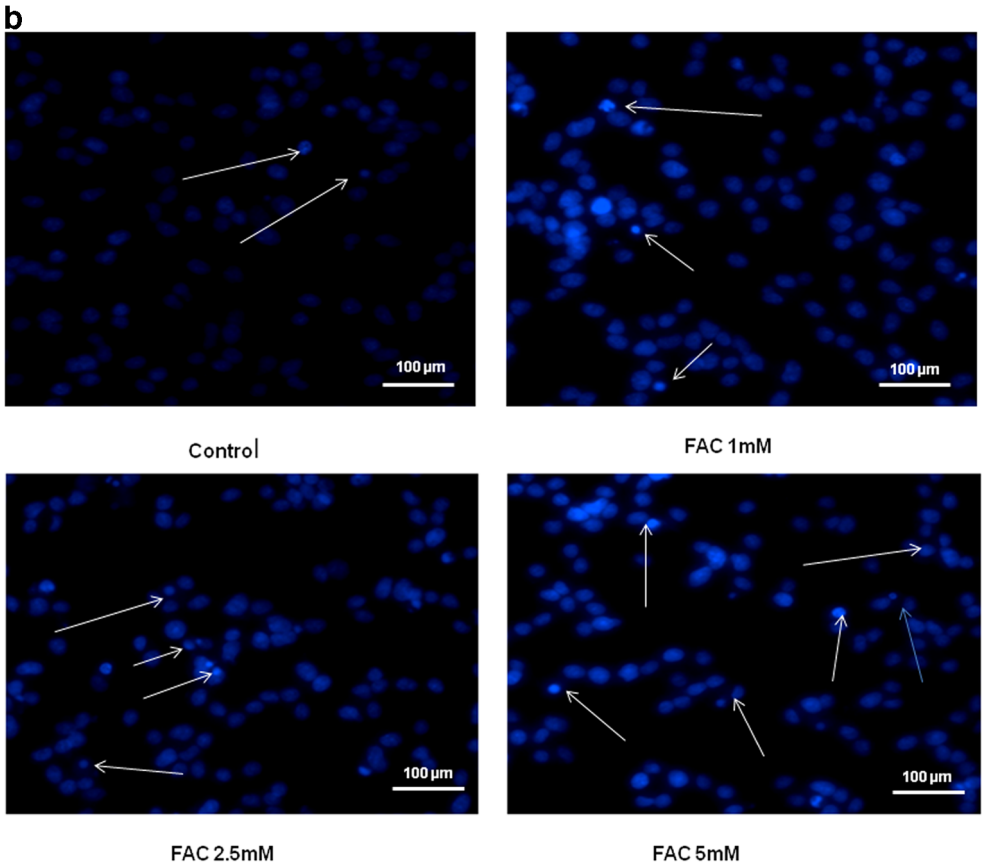

Fig. 4 (continued)

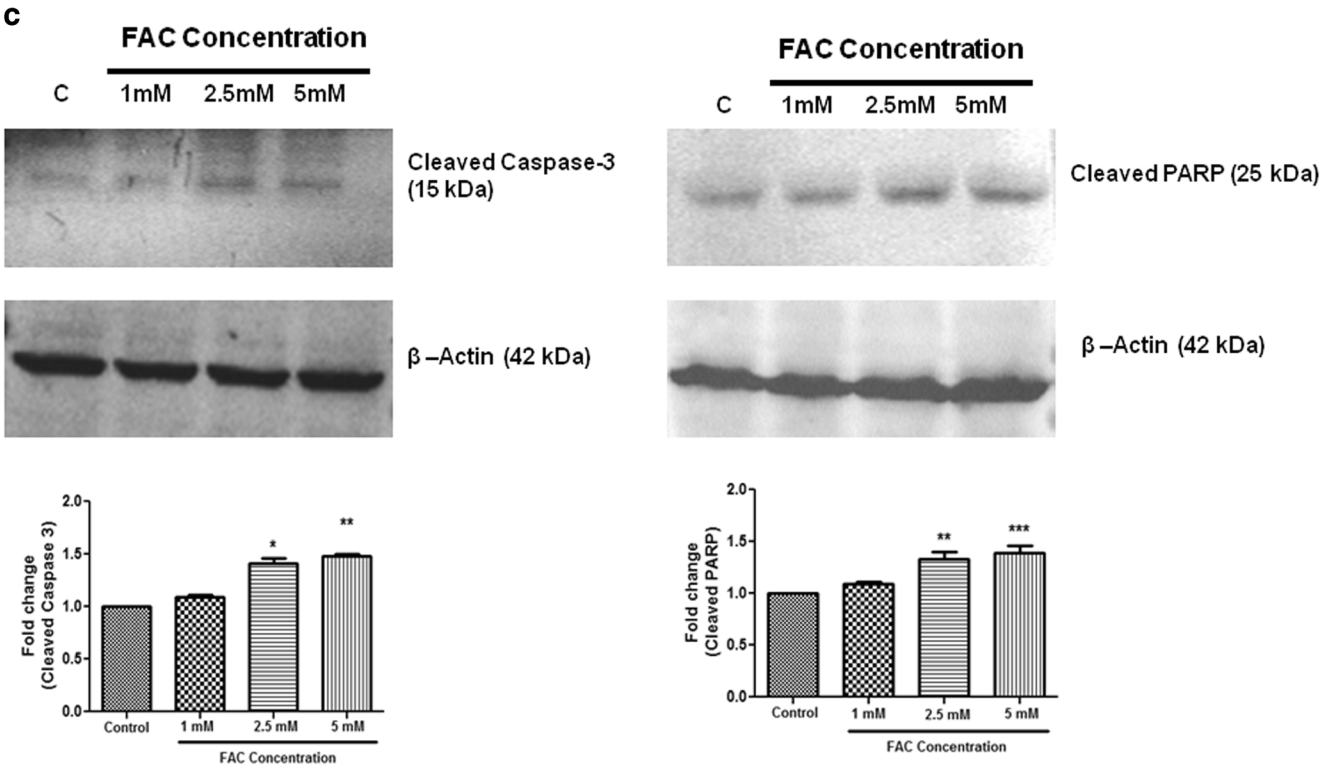

Fig. 4 (continued)

pathophysiological conditions in different vital organ systems like the hepatic system, cardiac system, and neuronal systems [12]. In the brain, availability of iron is tightly regulated by a sophisticated mechanism in order to exploit its utility in cellular operations, while preventing its deleterious effects. On the other hand, genetic mutation of Iron Regulatory Proteins (IRPs) may cause excess iron deposition which is sufficient to cause iron-elevated neurodegenerative diseases like Alzheimer's disease (AD) and Parkinson's disease (PD) [13]. However, the present investigation is an approach to understand the molecular mechanism and cell death pathways that are involved in iron-mediated neuronal cell deaths. With increasing doses of FAC (1 to 5 mM) on SH-SY5Y, neuroblastoma cells caused a dose-dependent gradual decrease in cell viability. Disappearance of neuritis and altered cellular morphology was further confirmed by bright-field microscopy. That iron decreased cell viability in primary cultures and as well as in SH-SY5Y cells were earlier demonstrated as described [14]. However, they conducted experiments using ferrous chloride as the iron source and at concentrations in micromolar levels.

Next, we intended to examine the effect of iron on the oxidative damage of cell, if any, through increased rate of ROS generation besides loss of mitochondrial membrane potential (MMP). Iron is an effective inducer for the generation of intracellular hydroxyl radicals (OH·) through the Fenton's reaction. In this study, it was indicated that the accumulation of iron increased the generation of intracellular ROS which prevailed over the cellular antioxidant mechanisms as customary, such as GSH and other free radical scavenging enzymes [15]. Decrease in MMP is the other evidence of altered mitochondrial activity and induction of the irreversible apoptotic cell death as a consequence of cellular oxidative damage [16].

Currently, ferroptosis is a well-studied phenomenon behind iron-mediated cell deaths which is highly dependent on the generation of oxidative stress but distinct from caspase-dependent apoptosis [17] and other forms of cell deaths. In the present study, it was also our interest to investigate if apoptosis was involved in the neuronal cell deaths that occurred as a consequence of iron treatment. A significant increase in early apoptotic and late apoptotic cells was observed and the data was highly correlated with the dose-dependent increase in FAC concentrations. Our results suggest that lower doses of FAC are sufficient to cause the early apoptosis of cells, and with increasing concentrations of FAC, the cells gradually moved into necrotic death following late apoptosis. Consequently, the condensation and fragmentation of nuclei with increased expression of cleaved casase-3 and cleaved PARP clearly signify the involvement of apoptotic pathways in iron-induced neuronal cell death [18–20].

Next, it was our interest to investigate the process of autophagy, if any, which could plausibly be involved in the cell death process. Taking into consideration again that cell death may be an outcome of interrupted autophagy, we treated SH-SY5Y cells with increasing doses of FAC, as prescribed, and further analyzed to determine the molecular events involved in

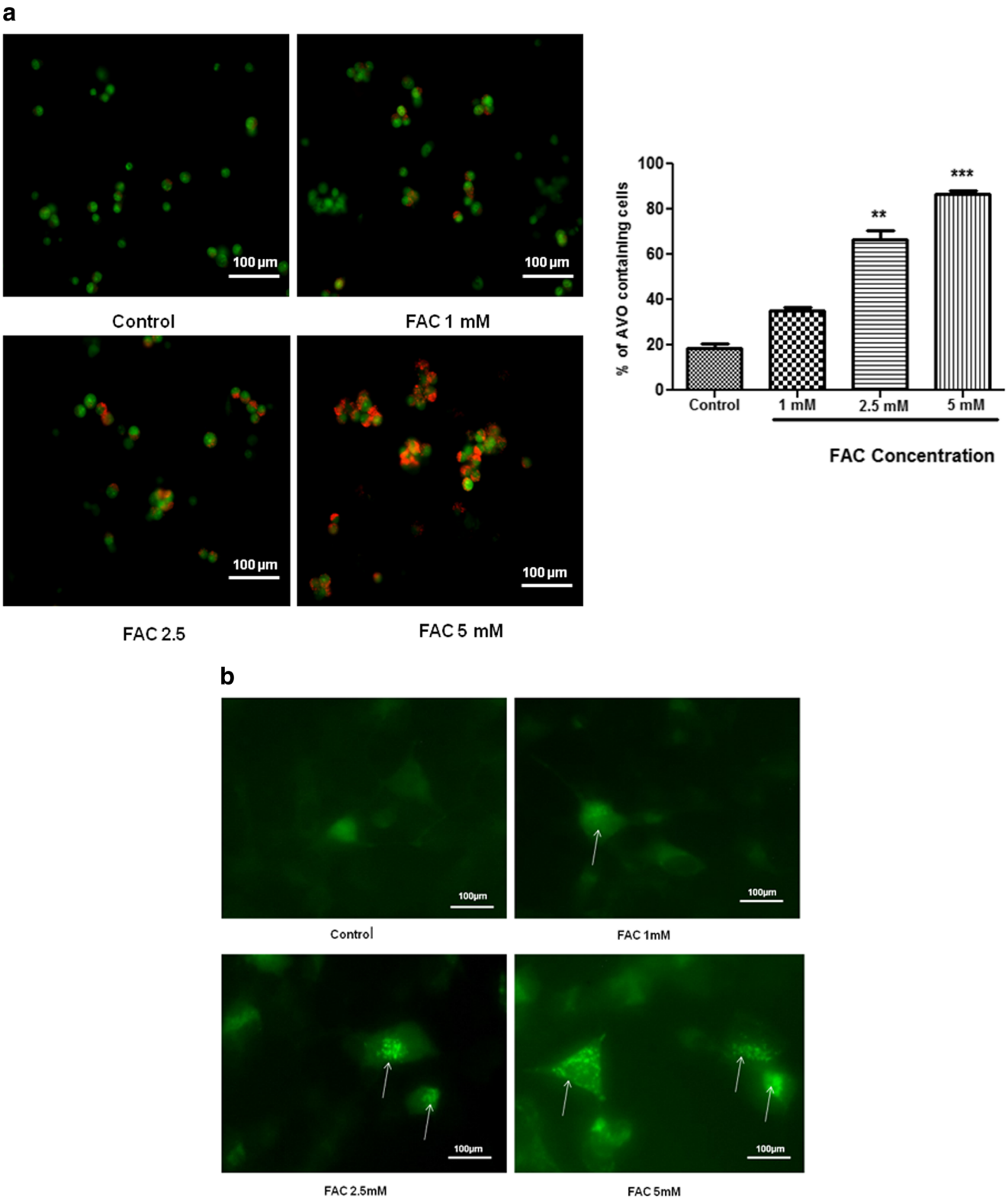

Fig. 5 Assessment of FAC-mediated autophagy induction. **a** Determination of AVO accumulation. AO stain was incorporated into the autophagosome and with increasing acidity; the gradual metachromatic shift from green fluorescence to red fluorescence is shown for 2.5 mM and 5 mM FAC treatments. All values were expressed as mean ± SD of three independent experiments [$^{**}P < 0.01$, $^{***}P < 0.001$ as compared with the untreated group (Control)]. **b** Determination of autophagosome accumulation. Fluorescence micrograph of LC3-GFP-transfected SH-SY5Y cells. Punctated LC3-GFP (white arrows) was observed in FAC-treated SH-SY5Y cells as compared with the diffused fluorescence of untreated cells. All experiments were performed in triplicate

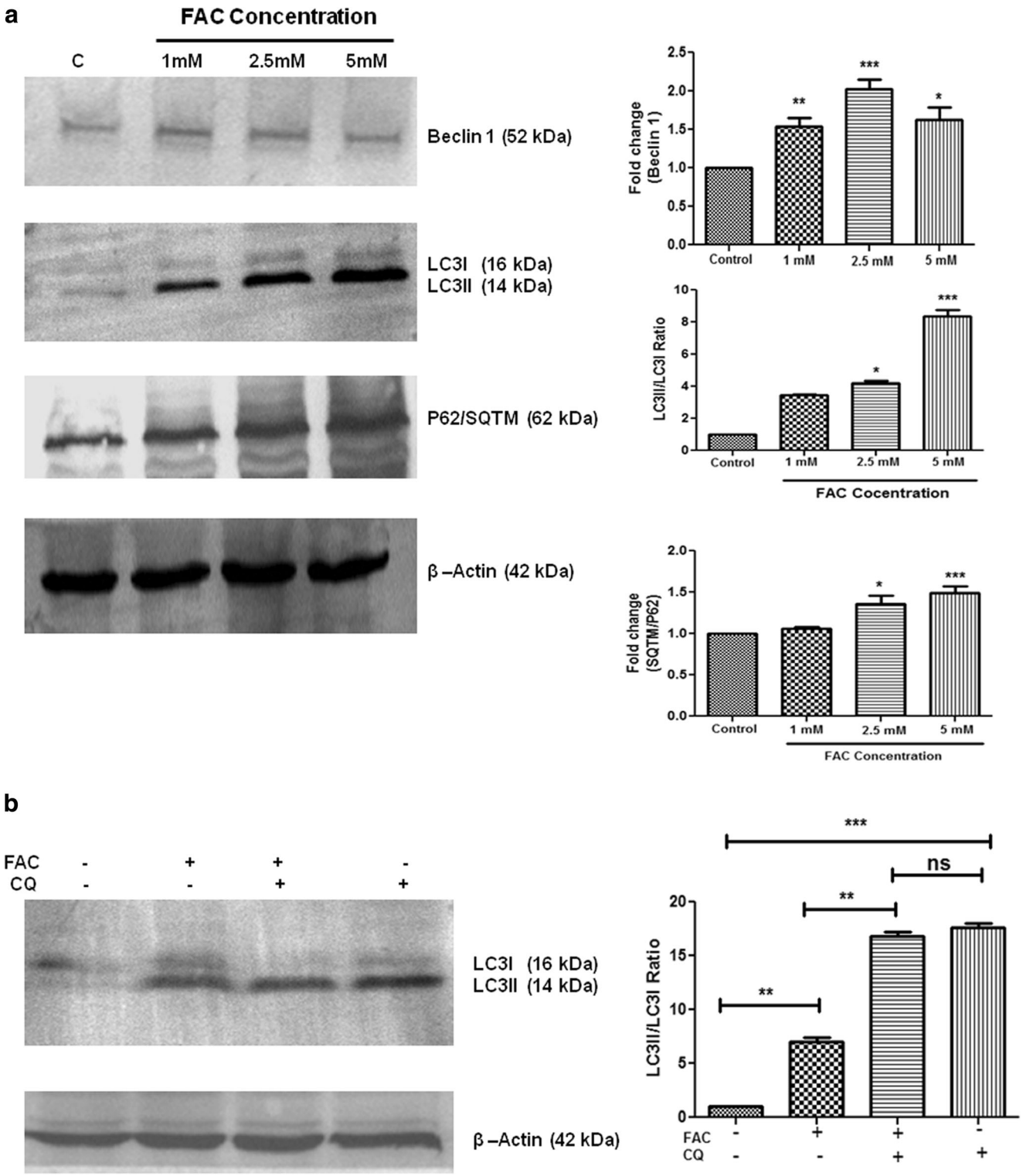

Fig. 6 Expressional study of autophagy marker proteins. **a** LC3I to LC3II conversion was clearly observed by means of Western blotting experiments with increasing doses of FAC. However, p62 expressions increased plausibly due to the inhibition of lysosomal degradation. The reduced amount of Beclin 1 expression as a result of higher doses of FAC compared with the lower FAC doses suggests no further autophagic progression. **b** LC3II expression was significantly increased in FAC (2.5 mM) treated and FAC with CQ-co-treated cells (**$P < 0.01$, ***$P < 0.001$ as compared with the Control). There is no significant (ns) change in LC3II expression level between CQ-treated and FAC with CQ-co-treated cells. The values were expressed as mean ± SD of three independent experiments [*$P < 0.05$, **$P < 0.01$, ***$P < 0.001$ as compared with the untreated group (Control, C)]

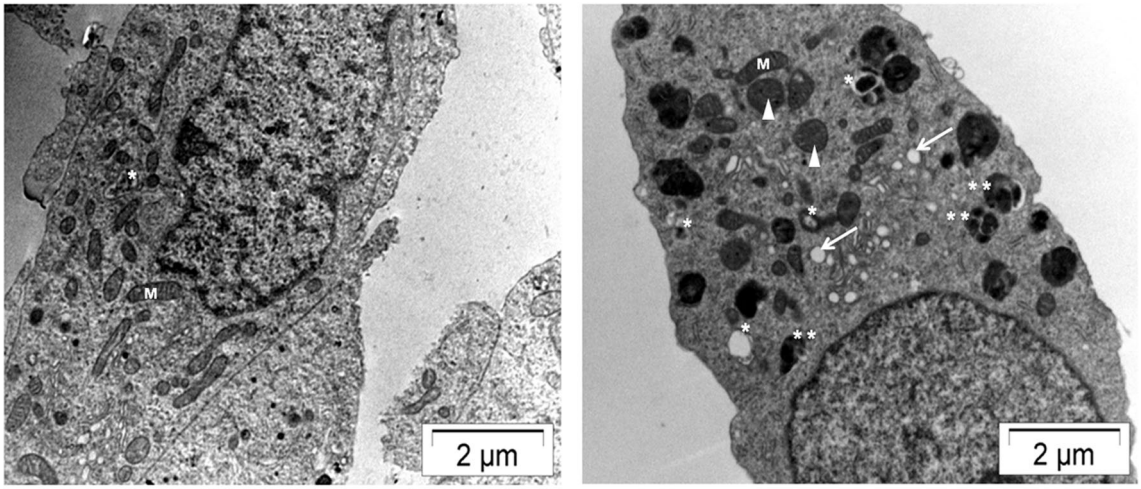

Fig. 7 Ultrastructural study revealed autophagy induction in FAC-treated SH-SY5Y cell line. As compared with the control cells, formation of autophagy-related structures was clearly seen in FAC-treated SH-SY5Y cells. Membrane-bound autophagic vacuoles (AV) (arrows), early autophagosomes (*), and late autophagosomes (**) were a clear evidence of FAC-mediated autophagy induction. Swollen mitochondria (arrow heads) were also observed in FAC-treated cells. M, mitochondria

the iron-mediated neuronal deaths. The autophagy pathway is known to be divided into three regulatory segments, viz. initiation or autophagosome formation, fusion of autophagosome and autolysosome, and finally the lysosomal degradations or termination. Inhibition in any of these events may lead to cell death [21]. In the present work, we used Acridine Orange (AO), a cell-permeable green fluorophore with increasing concentrations of FAC. In an acidic condition, as evident from the accumulation of acidic vesicular organelle (AVO) and as a consequence of autophagy progression, AO gets protonated resulting in a metachromatic shift from green to red fluorescence when compared with control cells. Concomitant with the AVO deposition, there was further LC3-GFP puncta formation observed as a marker of mature autophagosome formation. Further, the expression levels of other autophagy related genes, such as Beclin 1 and p62/SQTM1. Beclin 1 is an initiator protein of autophagy which is known to commence the phagophore formation [22]. Interestingly, Beclin 1 was found to be upregulated, as evidenced from the Western blotting studies suggesting once again a clear indication of autophagy initiation although there had been no significant increase in the initiator protein later with increasing doses of FAC. On the other hand, a different phenomenon was observed for the adaptor protein p62 expression, which is well known to degrade with the progression of autophagy [23]. Surprisingly, in the present investigation, the p62 levels remained unchanged for all FAC-treated cells in comparison with the controls. Besides, as expected, a twofold increase in the expression of LC3II concomitant with higher doses of iron was observed. Consequently, from the data obtained so far, it was clearly evident that the conversion of LC3I into its lipidated form, LC3II, was not sufficient to ascertain that there was indeed a progression of autophagy. However, our data establish the fact that initially a higher rate of autophagy was induced upon FAC treatment but resulted in an incomplete progression of the process possibly due to defects in late stage of autophagy [22, 24]. CQ is particularly a late stage autophagy blocker which is popularly known to inhibit lysosomal activity [25]. In the present study, co-treatment of FAC with CQ caused no significant increase in LC3 II expressional level as compared with the CQ-treated cell which confirms the blockage of autophagy in late stage. On the other hand, the presence of intracellular autophagic structures in FAC-treated SH-SY5Y cell lines were visualized by ultrastructual (TEM) studies which confirmed the induction of autophagy [26]. Moreover, the increased number of damaged or swollen mitochondria with augmented accumulation of AVs and APs in the cytoplasm is a clear indication of autophagic cell deaths [27].

Late stage autophagy inhibition is the outcome of lysosomal dysfunction. Lysotracker Deep Red staining revealed the formation of lysosomal acidic vesicles with an increase in size of lysosomes as compared with the control. Similar phenomenon was also observed in CQ-treated cells. Hence, it was evident that autophagy block was indeed due to the iron-induced lysosomal dysfunction. It was also evident that iron inhibited the lyosomal hydrolase activities [28, 29]. LC3-GFP-RFP reporter tracking is a well-accepted method to check the intracellular fate of LC3II during autophagy induction and also during autophagy block [30]. The presence of red fluorescence over the green fluorescence as a consequence of increasing iron treatment clearly signifies LC3B deposition which is correlated with lysosomal dysfunction [31].

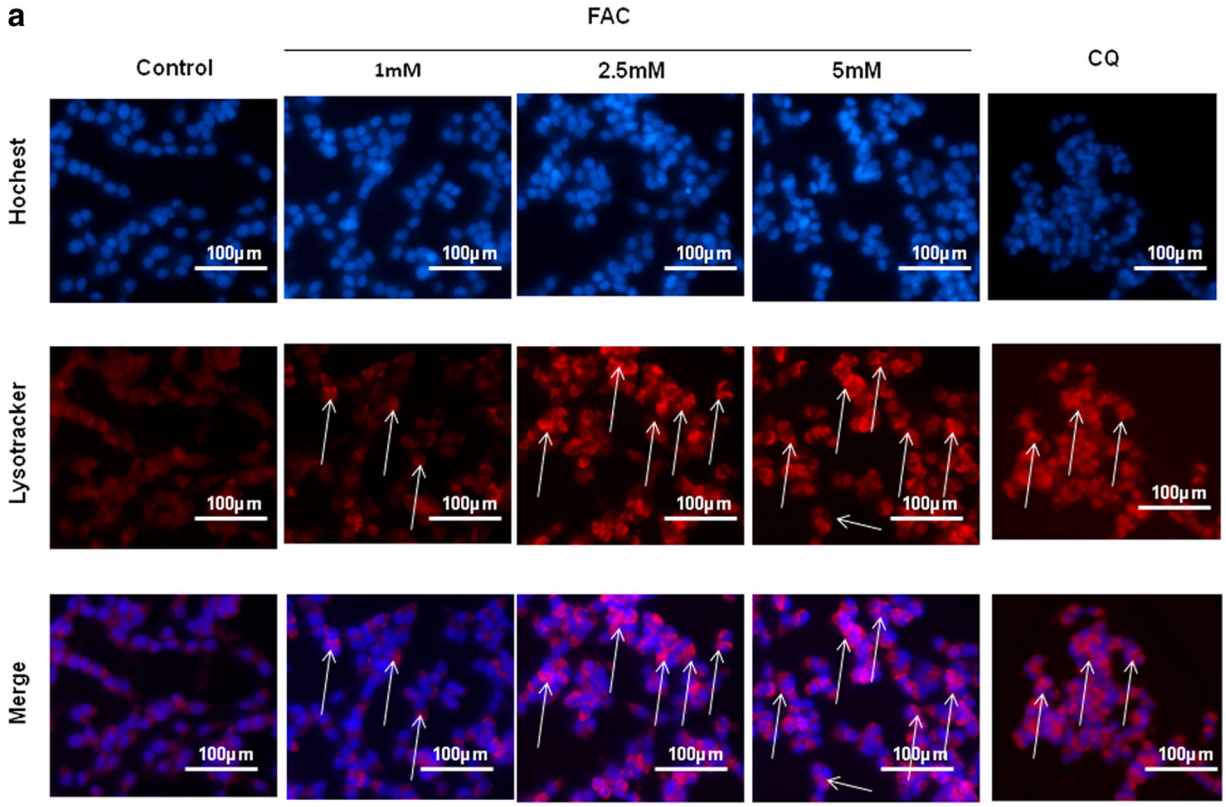
a
FAC
Control
1mM
2.5mM
5mM
CQ
Hochest
Lysotracker
Merge
100µm

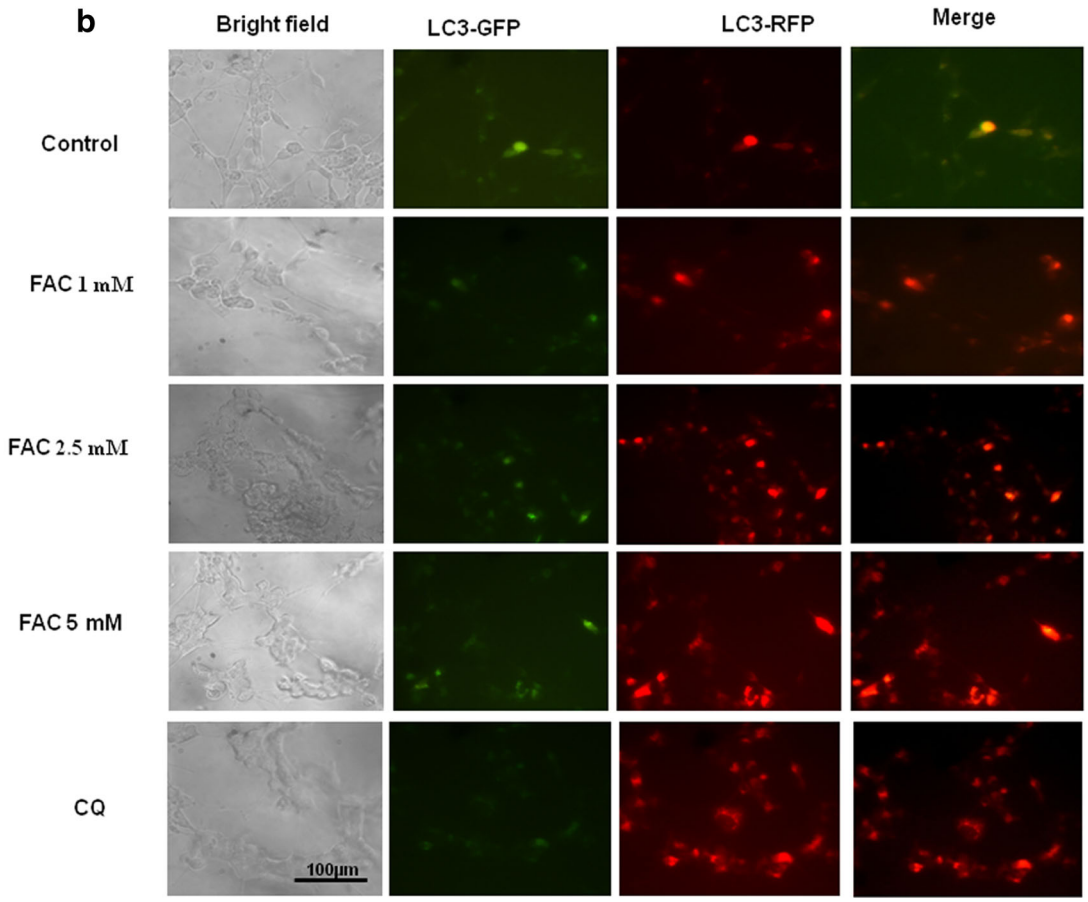
b
Bright field
LC3-GFP
LC3-RFP
Merge
Control
FAC 1 mM
FAC 2.5 mM
FAC 5 mM
CQ
100µm

◀ **Fig. 8** FAC induces the autophagy blocked. **a** FAC treatment and CQ treatment increased the incorporation of Lysotracker Deep Red stain as compared with the untreated cells. This suggests increased volume of lysosomes (white arrows) and not the numbers. **b** With increasing concentrations of FAC, LC3B-RFP was increased in comparison with the untreated cells, similar effect was observed in CQ treatment

Taken together, the present investigation attempts to focus that levels of iron are indeed crucial for maintaining the normal neuronal physiology but excess of iron deposition is sufficient to induce the generation of intracellular ROS leading to neuronal cell deaths. It was further evident that there was a significant correlation between increasing apoptotic cell populations with and enhanced population of AVO-containing cells which occurred as a result of high doses of FAC and subsequently caused the neuronal cell deaths. However, we report for the first time that interruption in autophagy progression or perhaps the inhibition of lysosomal hydrolase action is probably responsible for the iron-induced neuronal cell deaths. Our work thus demonstrates that iron-induced neuronal cell death is not only mediated by any apoptotic cell death pathway; death is induced through inhibition of autophagy pathway, which may be considered to be an alternative form of a cell survival pathway [32]. This work is intended to open new avenues in the field of treating iron-induced neurotoxicity that leads to neurodegeneration by inducing the progression of autophagy or completion of autophagy lysosomal pathway.

Acknowledgments JB gratefully acknowledges the financial support from the University Grants Commission (Major Research Project) No. 41-539/2012 (SR) and West Bengal University of Technology TEQIP II program for providing infrastructural facilities. JR is further thankful to ICMR SRF (No. 46/68/2015/BMS/TRM) for providing Senior Research Fellowship. SR acknowledges SERB for awarding the National Post Doctoral Fellowship (PDF/2017/001443). The authors are also thankful to Bose Institute, Kolkata, for providing the flow cytometry facilities and National Institute of Cholera and Enteric Diseases, Kolkata, for providing the TEM facilities.

Compliance with Ethical Standards

Conflict of Interest The authors declare that they have no conflict of interest.

References

1. Jaeger AP, Wyss-Coray T (2009) All-you-can-eat: autophagy in neurodegeneration and neuroprotection. Mol Neurodegener 4:16. https://doi.org/10.1186/1750-1326-4-16
2. Zhang Z, Miah M, Culbreth M, Aschner M (2016) Autophagy in neurodegenerative diseases and metal neurotoxicity. Neurochem Res 41:409–422. https://doi.org/10.1007/s11064-016-1844-x
3. Martinez-Vicente M (2015) Autophagy in neurodegenerative diseases: from pathogenic dysfunction to therapeutic modulation. Semin Cell Dev Biol 40:115–126. https://doi.org/10.1016/j.semcdb.2015.03.005
4. Spencer B, Potkar R, Trejo M, Rockenstein E, Patrick C, Gindi R, Adame A, Wyss-Coray T, Masliah E (2009) Beclin1 gene transfer activates autophagy and ameliorates the neurodegenerative pathology in alpha-synuclein models of Parinson's and Lewy body diseases. J Neurosci 29(43):13578–13588. https://doi.org/10.1523/JNEUROSCI.4390-09.2009.
5. Dixon SJ, Stockwell BR (2014) The role of iron and reactive oxygen species in cell death. Nat Chem Biol 10:9–17. https://doi.org/10.1038/nchembio.1416
6. Salvador GA (2010) Iron in neuronal function and dysfunction. BioFactors 36:103–110. https://doi.org/10.1002/biof.80
7. Wu Y, Li X, Xie W, Jankovic J, Le W, Pan T (2010) Neuroprotection of deferoxamine on rotenone – induced injury via accumulation of HIF-1α and induction of autophagy in SH-Y5Y cells. Neurochem Int 57:198–205. https://doi.org/10.1016/j.neuint.2010.05.008
8. Chen CW, Chen TY, Tsai KL, Lin CL, Yokoyama KK, Lee WS, Chiueh CC, Hsu C (2012) Inhibition of autophagy as a therapeutic strategy of iron-induced brain injury after hemorrhage. Autophagy 8:1510–1520. https://doi.org/10.4161/auto.21289
9. Castino R, Fiorentio I, Cagnin M, Giovia A, Isidoro C (2011) Chelation of lysosomal iron protects dopaminergic SH-SY5Y neuroblastoma cells from hydrogen peroxide toxicity by precluding autophagy and AKT dephosphorylation. Toxicol Sci 123:523–541. https://doi.org/10.1093/toxsci/kfr179
10. Kidane TZ, Sauble E, Linder MC (2006) Release of iron from ferritin requires lysosomal activity. Am J Phys Cell Physiol 291:C445–C455. https://doi.org/10.1152/ajpcell.00505.2005
11. Guo F, Liu X, Cai H, Le W (2017) Autophagy in neurodegenerative diseases: pathogenesis and therapy. Brain Pathol 28:3–13. https://doi.org/10.1111/bpa.12545
12. Kohgo Y, Ikuta K, Ohtake T, Torimoto Y, Kato J (2008) Body iron metabolism and pathophysiology of iron overload. Int J Hematol 88:7–15. https://doi.org/10.1007/s12185-008-0120-5
13. Hare D, Ayton S, Bush A, Lei P (2013) A delicate balance: iron metabolism and diseases of the brain. Front Aging Neurosci 5:34. https://doi.org/10.3389/fnagi.2013.00034
14. Wan W, Jin L, Wang Z, Wang L, Fei G, Ye F, Pan X, Wang C, Zhong C (2017) Iron deposition leads to neuronal α-synuclein pathology by inducing autophagy dysfunction. Front Neurol 8:1. https://doi.org/10.3389/fneur.2017.00001
15. Nunez MT, Munoz P, Tapia V, Esparza A, Salazar J, Speisky H (2004) Progressive iron accumulation induces a biphasic change in the glutathione content of neuroblastoma cells. Free Radic Biol Med 37:953–960. https://doi.org/10.1016/j.freeradbiomed.2004.06.005
16. Wadia JS, Chalmers-Redman RME, Ju WJH, Carlile GW, Phillips JL, Fraser AD, Tatton WG (1998) Mitochondrial membrane potential and nuclear changes in apoptosis caused by serum and nerve growth factor withdrawal: time course and modification by (−)-deprenyl. J Neurosci 18:932–947. https://doi.org/10.1523/JNEUROSCI.18-03-00932.1998
17. Dixon SJ, Lemberg KM, Lamprecht MR, Skouta R, Zaitsev EM, Zaitsev EM, Gleason CE, Patel DN, Bauer AJ, Cantley AM, Yang WS, Morrison B 3rd, Stockwell BR (2012) Ferroptosis: iron-dependent form of non-apoptotic cell death. Cell 149:1060–1072. https://doi.org/10.1016/j.cell.2012.03.042
18. Crowley LC, Marfell BJ, Waterhouse NJ (2016) Analyzing cell death by nuclear staining with Hoechst 33342. Cold Spring Harb Protoc 2016(9):pdb.prot087205. https://doi.org/10.1101/pdb.prot087205

19. Porter AG, Jänicke RU (1999) Emerging roles of caspase-3 in apoptosis. Cell Death Differ 6:99–104. https://doi.org/10.1038/sj.cdd.4400476
20. Chaitanya GV, Steven AJ, Babu PP (2010) PARP-1 cleavage fragments: signatures of cell-death proteases in neurodegeneration. Cell Commun Signal 8:31. https://doi.org/10.1186/1478-811X-8-31
21. Kroemer G, Levine B (2008) Autophagic cell death: the story of a misnomer. Nat Rev Mol Cell Biol 9:1004–1010. https://doi.org/10.1038/nrm2529
22. Glick D, Barth S, Macleod KF (2010) Autophagy: cellular and molecular mechanisms. J Pathol 221:3–12. https://doi.org/10.1002/path.2697
23. Tanida I, Waguri S (2010) Measurement of autophagy in cells and tissues. Methods Mol Biol 648:193–214. https://doi.org/10.1007/978-1-60761-756-3_13
24. Tanida I, Minematsu-Ikeguchi N, Ueno T, Kominami E (2005) Lysosomal turnover, but not a cellular level, of endogeneous LC3 is a marker for autophagy. Autophagy 1:84–91
25. Mauthe M, Orhon I, Rocchi C, Zhou X, Luhr M, Hijlkema KJ, Coppes RP, Engedal N, Mari M, Reggiori F (2018) Chloroquine inhibits autophagic flux by decreasing autophagosome-lysosomefusion. Autophagy. 14:1435–1455. https://doi.org/10.1080/15548627.2018.1474314
26. Kroemer G, Levine B (2008) Autophagic cell death: the story of a misnomer. Nat Rev Mol Cell Biol 9(12):1004–1010. https://doi.org/10.1038/nrm2527
27. Mizushima N, Yamamoto A, Matsui M, Yoshimori T, Ohsumi Y (2004) In vivo analysis of autophagy in response to nutrient starvation using transgenic mice expressing a fluorescent autophagosome marker. Mol Biol Cell 15:1101–1111. https://doi.org/10.1091/mbc.e03-09-0704
28. Pivtoraiko VN, Stone SL, Roth KA, Shacka JJ (2009) Oxidative stress and autophagy in the regulation of lysosome-dependent neuron death. Antioxid Redox Signal 11:481–496. https://doi.org/10.1089/ARS.2008.2263
29. Yoon YH, Cho KS, Hwang JJ, Lee SJ, Choi JA, Koh JY (2010) Induction of lysosomal dilatation, arrested autophagy, and cell death by chloroquine in cultured ARPE-19 cells. Invest Ophthalmol Vis Sci 51:6030–6037. https://doi.org/10.1167/iovs.10-5278
30. Hansen TE, Johansen T (2011) Following autophagy step by step. BMC Biol 20119:39. https://doi.org/10.1186/1741-7007-9-39
31. Tanida I, Ueno T, Kominami E (2008) LC3 and autophagy. Methods Mol Biol 445:77–88. https://doi.org/10.1159/000478626
32. Das G, Shravage BV, Baehrecke EH (2012) Regulation and function of autophagy during cell survival and cell death. Cold Spring Harb Perspect Biol 4:a008813. https://doi.org/10.1101/cshperspect.a008813